journal

J. Am. Ceram. Soc., 97 [1] 258–266 (2014)
DOI: 10.1111/jace.12650

Tetravalent Doping of CeO_2: The Impact of Valence Electron Character on Group IV Dopant Influence

D. E. P. Vanpoucke,[‡,§,†] S. Cottenier,[§,¶] V. Van Speybroeck,[§] I. Van Driessche,[‡] and P. Bultinck[‡]

[‡]Department of Inorganic and Physical Chemistry, Ghent University, Krijgslaan 281-S3, Ghent 9000, Belgium

[§]Center for Molecular Modeling, Ghent University, Technologiepark 903, Zwijnaarde 9052, Belgium

[¶]Department of Materials Science and Engineering, Ghent University, Technologiepark 903, Zwijnaarde 9052, Belgium

Fluorite CeO_2 doped with group IV elements is studied within the density functional theory (DFT) and DFT + U framework. Concentration-dependent formation energies are calculated for $Ce_{1-x}Z_xO_2$ (Z = C, Si, Ge, Sn, Pb, Ti, Zr, Hf) with $0 \leq x \leq 0.25$ and a roughly decreasing trend with ionic radius is observed. The influence of the valence and near valence electronic configuration is discussed, indicating the importance of filled d and f shells near the Fermi level for all properties investigated. A clearly different behavior of group IVa and IVb dopants is observed: the former are more suitable for surface modifications and the latter are more suitable for bulk modifications. For the entire set of group IV dopants, there exists an inverse relation between the change, due to doping, of the bulk modulus, and the thermal expansion coefficients. Hirshfeld-I atomic charges show that charge-transfer effects due to doping are limited to the nearest-neighbor oxygen atoms.

I. Introduction

Over the last two decades, interest in ceria-based materials has grown steadily. The facile $Ce^{4+} \leftrightharpoons Ce^{3+}$ redox conversion in combination with the fact that CeO_2 retains its fluorite crystal structure even with significant degrees of reduction makes ceria-based materials ideal for controlling the oxygen atmosphere in three-way catalysts.[1–4] Furthermore, the introduction of dopants such as Zr has been shown to increase the oxygen storage capacity, increasing the range of practical applicability.[5] The remarkable redox properties of CeO_2 make ceria-based materials also of interest in several other industrially important applications, such as: catalytic support, thermal barrier coatings, ionic conductors, and fuel cells.[6–9] More recently, CeO_2 and ceria-based materials have been used as thin film buffer layers in $YBa_2Cu_3O_{7-\delta}$-coated superconductors.[10–16]

For all these applications, there is a constant search for ways to improve the properties of ceria-based materials even further. One of the most common ways for such improvements is through the introduction of dopants, with regimes ranging from light doping (<1%) to mixed oxides containing 50% dopants or more.[1,17] In addition, different applications also require different properties to be optimized. Unfortunately, optimization toward one application may worsen the performance of the system for another. As an example, for ionic conductors one wishes to maximize the ionic conductivity, whereas for a buffer layer one often wishes to minimize this quantity. Such opposing and varying requirements make a more general theoretical study of the influence of dopants on the properties of CeO_2 of general interest. This is the particular aim of the present article.

Experimentally, lanthanide elements are most often studied as dopants, in addition to standard catalyst d-block metals (Au, Pd, Cu, etc.,).[1,3,7,8,17–31] As all these elements can act as aliovalent dopants, charge compensating oxygen vacancies are introduced, contributing to the changes in the CeO_2 properties. To have a clear understanding of the influence dopants have on the properties of CeO_2, it is important to separate the contributions of these two structural changes; i.e., to distinguish between the consequences of doping and the subsequently introduced charge compensating vacancies. Theoretical calculations are ideally suited to separate the different contributions. Due to the tetravalent nature of Ce in CeO_2, group IV elements are the perfect starting point for such investigations.

Only few studies addressed group IV dopants in ceria-based materials, although for example silica is a widely used catalyst support.[32,33] This limited experimental work originates from the difficulty of forming solid solutions with CeO_2 in a controlled way. Improved redox properties compared with pure and Zr-doped CeO_2 have been presented for mixed CeO_2–SiO_2 and CeO_2–SnO_2 materials.[32,34–36] Andersson *et al.* studied the redox properties of tetravalent dopants at low dopant concentrations of 3% and found a correlation between the reducibility and the dopant's ionic radius.[37,38] Tang *et al.* investigated the redox properties of tetravalent dopants (Mn, Pr, Sn, and Zr) and linked the lower oxygen vacancy formation energy to structural distortions and electronic modifications.[39] Yashima studied tetragonal crystal phases of $Ce_{1-x}Zr_xO_2$ and found a tetragonal phase to appear for Zr concentrations ≥37.5%, and a cubic phase with displaced O atoms at lower concentrations.[40] We previously found Vegard law behavior for group IV-doped CeO_2 and proposed the Shannon crystal radius instead of the ionic radius as parameter for the lattice expansion.[41]

In this article, we investigate the modification in the mechanical properties of CeO_2 due to doping with group IV elements using density functional theory (DFT). We show there is a difference in energetics for doping between group IVa and IVb elements, and link this to the different valence electronic structure [Section II*(1)* and *(2)*]. An inverse relation between the bulk modulus (BM) and the thermal expansion coefficients (TECs) is presented [Section II*(3)*] and the change in the charge distribution around the dopants discussed [Section II*(4)*]. Technical details of the computational methods used are provided in Appendix A.

I. Tanaka—contributing editor

Manuscript No. 32620. Received January 30, 2013; approved September 2, 2013.
†Author to whom correspondence should be addressed. e-mail: danny.vanpoucke@ugent.be

II. Results and Discussion

(1) Defect Formation Energies

The stability of the different group IV-doped fluorite CeO_2 systems is investigated through the comparison of the defect formation energies E_f, which are calculated as follows:

$$E_f = E_{Ce_{1-x}Z_xO_2} - E_{CeO_2} + N_{df}(E_{Ce} - E_Z) \quad (1)$$

with N_{df} the number of substituent atoms in the system, $E_{Ce_{1-x}Z_xO_2}$ the total energy of the relaxed-doped system, E_{CeO_2} the total energy of a CeO_2 fluorite supercell of equal size, E_{Ce} and E_Z the energy per atom of bulk α-Ce and the bulk phase of the substituent element Z. Larger positive values of E_f indicate that more energy is required for doping. Pure Ce metal has several different phases depending on the external pressure and temperature. In our case, we chose to use the α-phase, as the calculations are performed at zero temperature and pressure. The used crystal structure of the dopant element bulk phase is presented in Appendix A, Table V. Defect formation energies can also be calculated with regard to dopant-oxides, and are presented in Appendix B. The obtained results remain qualitatively the same as those presented below.

Table I shows that E_f varies only slightly with dopant concentration. For cells with a dopant concentration of 3.125% E_f is also calculated within the DFT + U framework, using the local density approximation (LDA)/Perdew, Burke, and Ernzerhof (PBE) optimized geometry and a Hubbard U = 5 eV for the Ce f electrons. As can be seen in Table I, the formation energies are slightly larger in the DFT + U framework, although they do not change the relative stability of the systems compared with the pure LDA/PBE results.

For different substituent elements, the formation energies show a spread over quite a large range, with roughly 20 eV/atom required to imbed a C atom, down to merely 0.1 eV/atom required to imbed a Hf atom. This shows that none of the group IV elements increase the stability of CeO_2. A direct comparison with experiment is not straightforward, as *ab initio* calculations do not account for effects of pressure and temperature. In addition, during the experimental preparation of a compound there are often several steps (thermal and/or mechanical treatment, etc.,) involved which provide additional energy to the system that enable the formation of metastable-doped systems. For example, in experiments one observes that oxygen vacancies form spontaneously in CeO_2 cubic fluorite,[1] although *ab initio* simulations show them always to require energy. In an attempt to compare with experiment, we use our calculated oxygen vacancy formation energy as a reference. Substitutions that require the same *ab initio* computed energy as this reference, or less, are considered more likely under experimental conditions, while those requiring more, less likely. For the LDA and PBE functionals, we calculated the O vacancy formation energy to be 4.035 and 3.097 eV per vacancy, respectively, at a vacancy concentration of 1.5625%, in excellent agreement with values found in literature.[42,43] Comparing the 4.035 eV found for pure LDA to the 3.61 eV for LDA + U presented by Andersson *et al.*,[42] shows that the introduction of a Hubbard U term does not qualitatively alter the stability difference observed for the group IVa and IVb dopants. Note, however, that the pure LDA value is closer to the experimental value of 4.65–5.00 eV for bulk reduction.[44] For higher O vacancy concentrations higher formation energies are found, up to 5.006 and 4.145 eV for LDA and PBE, respectively, at 12.5%, which is within the range of experimentally derived values.[44]

Based on these reference energies, the dopants in Table I nicely split in the "more likely bulk dopants" (group IVb) and the "less likely bulk dopants" (group IVa). In this context, group IVb dopants are likely to remain (homogeneously) dispersed in the bulk of the CeO_2 grains and crystals, whereas the group IVa dopants would likely segregate to the surface regions of the CeO_2 grains, or the interface regions with other materials, or cluster to form small domains of the dopant element inside CeO_2 crystals and grains. This makes the latter of interest for applications where tuning of surface effects is important. The former, however, are expected to remain distributed in the CeO_2

Table I. Defect Formation Energy for Group IV Dopants at Different Concentrations

	E_f (eV)				
	25%	12.5%	3.704%	3.125%	3.125%
			LDA		LDA + U[†]
CeO_2			−11.484[‡]		–
C	20.435	20.654	20.747	20.748	21.088
Si	8.288	8.078	8.050	8.052	8.358
Ge	9.404	9.134	9.110	9.105	9.341
Sn	7.061	6.866	6.851	6.851	7.013
Pb	8.963	8.757	8.742	8.745	8.866
Ti	3.168	3.254	3.248	3.233	3.563
Zr	0.530	0.555	0.548	0.543	0.796
Hf	0.105	0.139	0.131	0.128	0.392
			PBE		PBE + U[†]
CeO_2			−10.418[‡]		–
C	19.687	19.889	19.954	19.967	20.143
Si	8.737	8.547	8.530	8.562	8.764
Ge	9.495	9.257	9.242	9.254	9.386
Sn	7.129	6.967	6.962	6.960	7.031
Pb	8.960	8.788	8.777	8.780	8.812
Ti	3.454	3.526	3.524	3.532	3.740
Zr	0.851	0.884	0.885	0.883	1.033
Hf	0.484	0.517	0.517	0.517	0.666

[†]For the DFT + U calculations a Hubbard U = 5 eV was chosen both for the LDA and PBE calculations.
[‡]Instead of the formation energy the heat of formation is given.

bulk, making them well suited for applications where CeO_2 bulk parameters need to be modified, or in oxide mixing experiments. These results also agree with the observation that Zr-doped CeO_2 is widely used and easily produced in experiments, whereas it is much harder to form Si- and Sn-doped CeO_2 in a controlled way.[32,34–36]

For the group IVb elements, the formation energy decreases with increasing atomic size, showing a better size-match with Ce results in reduced system strain.[41] The formation energies for the group IVa-doped systems show a similar globally decreasing trend. The additional oscillation is interesting, and is retained even with the introduction of the Hubbard U correction. The slight increase in the formation energy for Ge and Pb coincides with the introduction of a "new" filled shell, the d shell in case of Ge, and the f shell in case of Pb. This shows that not only the outer valence electrons play a role in the stability of the system but also the presence of filled shells near the Fermi level.

(2) Density of States

We investigated the influence, at low concentration (x = 3.125%), of group IV dopants on the density of states (DOS) of $Ce_{1-x}Z_xO_2$, within the DFT + U framework. Due to the low concentration, the general shape of the DOS is comparable to the DOS of pure CeO_2; there is a conduction band of unoccupied Ce 4f states in the band gap between the O 2p valence band and Ce 5d conduction band (e.g., Figs. 1 and 2). Table II shows that the band gap between the unoccupied Ce 4f states and the O 2p valence band is always smaller than for

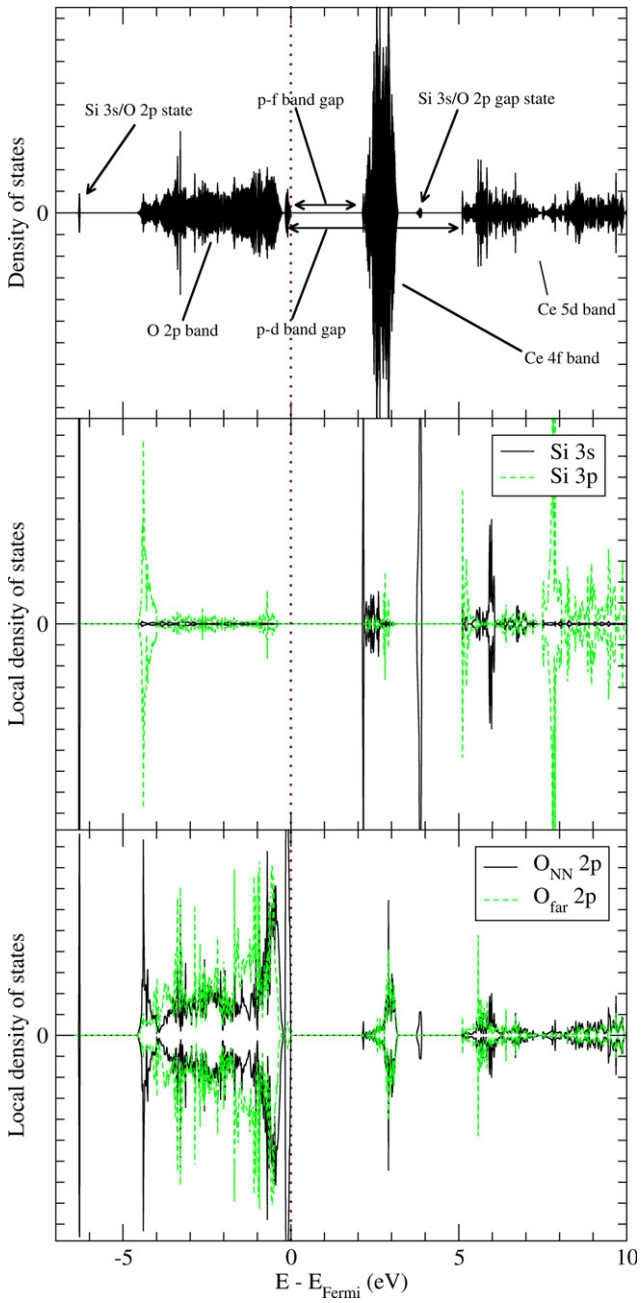

Fig. 1. The total DFT + U DOS for $Ce_{0.96875}Si_{0.03125}O_2$, indicating important features (top). The 3s and 3p Si LDOS, showing the origin of the gap state and atomic state below the O 2p band (middle). The 2p O LDOS for the eight nearest-neighbor (NN) O atoms surrounding the Si dopant, and an O atom far away from the dopant (bottom). The upper and lower panels present the spin up and spin down channels, respectively.

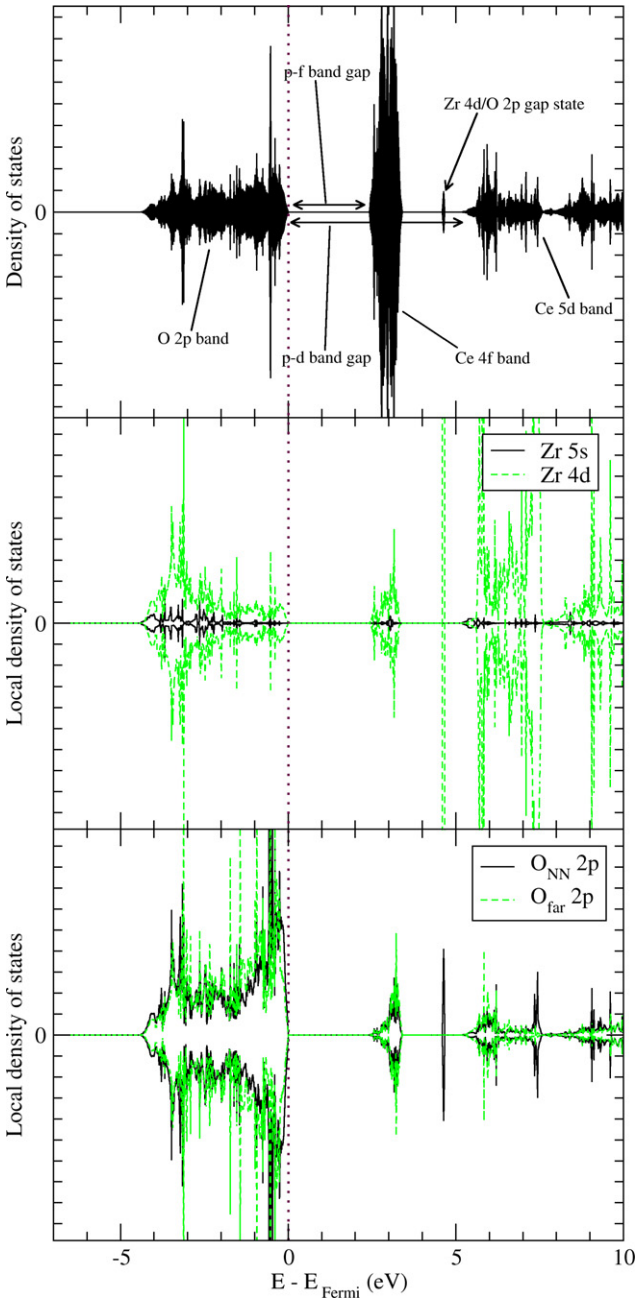

Fig. 2. The total DFT + U DOS for $Ce_{0.96875}Zr_{0.03125}O_2$, indicating important features (top). The 5s and 4d Zr LDOS, showing the origin of the gap state and atomic state below the O 2p band (middle). The 2p O LDOS for the eight nearest-neighbor (NN) O atoms surrounding the Zr dopant, and an O atom far away from the dopant (bottom). The upper and lower panels present the spin up and spin down channels, respectively.

Table II. Band Gaps in Group IV-doped CeO_2[†]

	LDA + U			PBE + U		
	2*p* 4*f*	2*p* 5*d*	*gs*	2*p* 4*f*	2*p* 5*d*	*gs*
CeO_2	2.45	5.35	–	2.37	5.35	–
C	2.26	5.18	−0.17	2.12	5.14	−0.21
Si	2.14	5.11	3.87	2.06	5.10	3.62
Ge	2.24	5.16	1.80	2.18	5.19	1.67
Sn	2.30	5.25	3.88	2.22	5.26	3.65
Pb	2.38	5.29	1.79	2.29	5.29	1.61
Ti	2.36	5.02	4.18	2.27	5.05	3.82
Zr	2.42	5.19	4.63	2.33	5.19	4.44
Hf	2.41	5.48	5.37	2.32	5.43	5.25

[†]Size of the $Ce_{1-x}Z_xO_2$ (with $x = 0.03125$) band gaps between the O 2*p* and Ce 4*f* bands and between the O 2*p* and Ce 5*d* bands (cf. Figs. 1 and 2). The position of the gap state (*gs*) with regard to the valence band edge is given for the group IVa elements (*s* state), and the group IV *b* elements (*d* state). All values are given in eV.

Table III. Calculated Bulk Moduli and Thermal Expansion Coefficients for Group IV-Doped CeO_2[†]

	B_0 (Mbar)		α (10^{-6} K^{-1})	
	LDA	PBE	LDA	PBE
CeO_2	2.017	1.715	11.218	12.955
C	1.528	1.235	16.287	20.379
Si	2.057	1.738	12.335	14.994
Ge	1.909	1.573	14.390	18.454
Sn	2.004	1.692	12.157	14.357
Pb	1.845	1.516	14.006	17.715
Ti	2.145	1.825	11.195	12.971
Zr	2.153	1.878	10.960	12.212
Hf	2.194	1.881	10.652	12.146

[†]The bulk modulus (BM) B_0 for CeO_2 is calculated for a dopant concentration of 25%. The linear TEC α is calculated at the same dopant concentration and a temperature of 500 K. The full TEC curves are shown in Fig. 3.

pure CeO_2. Excluding C, we find for both group IVa and IVb dopants an increase in the band gap size with the atomic number (within each group). The same behavior is observed for the O 2*p*–Ce 5*d* band gap. Comparison of the LDA + U and PBE + U results in Table II, shows that the trends are independent of the functional used. In case of the group IVa elements, there is an atomic band roughly 2 eV below the O 2*p* band (e.g., Fig. 1). From the local DOS (LDOS), it is clear that this localized state is a combination of the dopant *s* state and the O 2*p* state of the O ions surrounding the dopant. This is shown for Si doping in Fig. 1, and agrees well with the work of Andersson *et al.*[37] where a symmetry broken configuration was studied. In contrast to that work, we also observe such a localized combined state in the 2*p*–5*d* band gap (cf., Fig. 1). Closer investigation reveals that both bands each integrate to two electrons, indicating that this is a pair of bonding and antibonding states. To investigate this discrepancy the LDOS for a symmetry broken configuration ($Ce_{0.96875}Si_{0.03125}O_2$) was calculated. With the exception of the Ce 4*f* gap state, due to the presence of an oxygen vacancy in the structure of Andersson *et al.*,[37] we obtained qualitatively the same LDOS as was reported by these authors. This indicates that our observed *s*–*p* gap state originates from the different chemical environment for the Si dopant. However, it remains unclear to us if this state simply vanished upon symmetry breaking, or merely merged with the Ce 5*d* band. The work of Tang *et al.* on Sn-doped CeO_2 also shows the appearance of such atomic states below the O 2*p* band and in the band gap.[39] Furthermore, Tang *et al.* show that the gap state lies under the Fermi level when an oxygen vacancy next to the dopant is created, showing the excess electrons to transfer to the group IVa dopant. Table II shows the position of these gap states with regard to the valence band edge. This shows that only for C doping this state is occupied and is located at the edge of the valence band (hence the negative value). For the other IVa elements, the band is either located above or below the unoccupied Ce 4*f* band. The relation between these gap states and the atomic state below the O 2*p* valence band becomes even clearer due to the strong correlation of their position, placing the atomic states for the Ge- and Pb-doped systems roughly 0.7 eV below those of the Si- and Sn-doped systems.

In the LDOS of the heavier group IVa, elements also filled *d* (Ge, Sn) and *f* (Pb) states near the Fermi level are observed, in line with the behavior expected from the calculated formation energies (cf., Table I), gap state positions (cf., Table II), and mechanical properties (cf., Table III).

For the group IVb elements no atomic state below the O 2*p* valence band is present, only a gap state above the unoccupied Ce 4*f* band is observed (e.g., Fig. 2). This state moves toward the Ce 5*d* band, with increasing ionic size of the dopant (cf., Table II). For the Ti and Zr dopants, the band integrates to six and four electrons, respectively. In case of the Hf dopant this band shows a small overlap with the Ce 5*d* band, and the number of electrons is estimated to be in the range of that found in Ti- and Zr-doped ceria. Just as for the IVa elements, this localized state is a combination with O 2*p* states of the O ions surrounding the dopant, as is shown for Zr in Fig. 2.

In addition, the DOS and LDOS of systems with a dopant concentration of 25% were investigated within the pure DFT framework. We found qualitatively similar results, showing the presence of *d* and *f* states just below the Fermi-level for group IVa dopants with filled *d* and *f* shells.

For the group IVa dopants (except C), the presence of *s*-type conduction states results in a serious reduction in the 2*p*–4*f* band gap, compared with the low concentration systems. Furthermore, the position of the maximum of these *s* bands appears correlated with the defect formation energies.

In case of the group IVb dopants, on the other hand, the 2*p*–4*f* band gap does not change with the dopant concentration. Similar as for the low concentration systems, the unoccupied Ce 4*f* band contains a significant contribution of the group IVb dopant *d*-state (cf. Fig. 2).

As a result, the clearly better stability of the group IVb-doped systems, may be attributed to the better resemblance of the dopant LDOS to the LDOS of Ce. In addition, the reduction in the 2*p*–4*f* band gap width in the group IVa-doped systems, and its correlation with the defect formation energy suggests that either the 2*p*–4*f* band gap is important for the stability of the system, or that the presence of *s* states near the Fermi-level is detrimental for its stability.

(3) Thermal Expansion Coefficients and Bulk Moduli

We investigated the influence of group IV dopants on the mechanical properties of CeO_2, more specifically, the TEC and the BM. To reduce the computational cost, cells with a dopant concentration of 25% are used.

The linear (α) and volumetric (β) TECs of the doped systems can clearly be distinguished, as is seen in Fig. 3. Although group IVa dopants result in a significant increase in the TEC, group IVb dopants result in a status quo or a very small decrease in the CeO_2 TEC. In Table III, the calculated BM and linear TEC at 500 K of doped CeO_2 are compared, as both the TEC and the BM give a measure for how easily a material deforms under external conditions. Doping of CeO_2 only has a small influence on the system's BM, except for C. As experimentally most often lower concentrations are used, even a smaller influence is expected.

Similar as for the defect formation energies, an oscillation is seen for the BM and TEC values of group IVa-doped

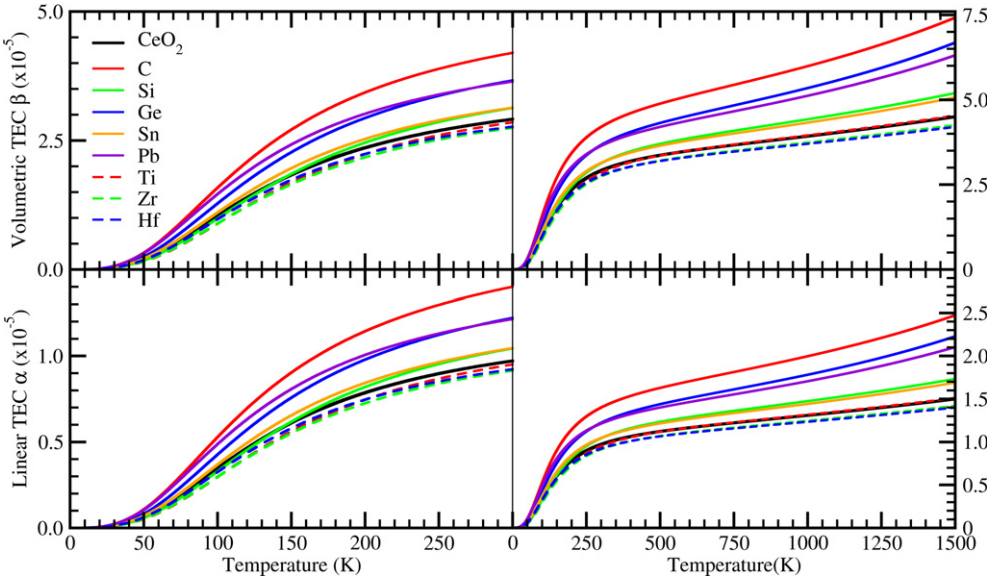

Fig. 3. Volumetric (top) and linear (bottom) TECs for LDA calculations. The left panels zoom in on the 0–300 K interval, the right panels show the same data over a 0–1500 K interval. Dopant concentrations of 25% are used.

ceria, showing the importance of filled *d* or *f* shells near the Fermi-level. For the group IVa elements, either the introduction of a filled *d* or *f* shell near the Fermi-level or the gap states in the O 2*p*–Ce 4*f* band gap reduces the resistance to compression (i.e., lower BM).

Comparison of the BMs and TECs in Table III shows an inverse relation between the two: an increase in the BM corresponds to a decrease in the TEC, and *vice versa*. However, the relative positions of Si and Sn appear reversed, as do those of Ge and Pb. Examining the TEC curves presented in Fig. 3 shows that around 250 K the order of the Si and Sn curves switches (the same for Ge and Pb), restoring the inverse behavior of the TEC and BM for the group IVa elements at lower temperatures. Because the BM is calculated at 0 K the trend of the inverse behavior is found to be a general one. These findings agree with our expectations: First, as the BM is a measure of the resistance of a material against uniform compression/expansion, it stands to reason that a large BM will lead to a small TEC. Second, it is well-known that both the BM and cohesive energy relate to the melting temperature, implying that the BM and cohesive energy correlate as well.[45] On the other hand, the linear TEC α and the cohesive energy show an inverse correlation.[46] As a result, an inverse correlation between the BM and linear TEC α is expected.

For practical applications, e.g., to reduce interfacial strain in a layered system through BM matching of the different layers,[15] a linear interpolation of the presented BM could be used to obtain a first-order approximation of the optimal dopant concentration.[41] For the elements of group IVb, Table III shows a BM that is only slightly larger than that of CeO_2 and that increases with the dopant atomic number. The group IVa elements show a more complex behavior (cf., above), and with the exception of Si, all lower the BM of CeO_2. As a result, group IV elements are not suitable as dopants if an increase in the CeO_2 BM is required. However, group IVa elements could be beneficial to obtain a lowered BM. In addition, the nature of the group IVa elements [cf., Section II*(1)*] may limit the effects to the grain boundaries or interfaces, allowing one to create a BM gradient using group IVa-doped CeO_2.

(4) Atomic Charges and Charge Transfer

The introduction of dopants in CeO_2 not only influences the electronic structure at the level of bands and the DOS but also at the level of the local charge density distribution. To investigate this effect we calculate the atomic charges in the doped systems using the Hirshfeld-I method.[47–49] Table IV shows the calculated charges on the dopant elements. The charge of the O and Ce atoms in pure CeO_2 is shown as reference.

Table IV. Hirshfeld-I Charges in $Ce_{1-x}Z_xO_2$, with Z a Group IV Element†

	M	O		Ce	
		NN	Far	NNN	Far
CeO_2	–	−1.41		2.81	
C	0.94	−1.17	−1.41	2.79	2.81
Si	2.23	−1.30	−1.41	2.79	2.81
Ge	2.33	−1.31	−1.41	2.79	2.81
Sn	2.64	−1.37	−1.41	2.80	2.81
Pb	2.49	−1.36	−1.41	2.80	2.81
Ti	2.65	−1.37	−1.41	2.80	2.81
Zr	2.97	−1.42	−1.41	2.81	2.81
Hf	3.03	−1.42	−1.39	2.80	2.80

†Calculated Hirshfeld-I atomic charges for $Ce_{1-x}Z_xO_2$ with $x = 3.125\%$ using LDA charge density distributions. All values are in *e*. The first column gives the atomic charge of the dopant Z. With regard to the dopant atom the shell of nearest and next nearest-neighboring atoms (NN and NNN) consist entirely of O and Ce, respectively. The respective positions are shown in Fig. 4 The atomic charges of these atoms are compared with the charges of O and Ce atoms at a longer distance (indicated as "far").

The atomic charges for all dopants show an increase of no more than 0.05*e* when increasing the dopant concentration from 3.125% to 25%. This is a first indication that the influence of the dopants on the electron density distribution is quite localized. Mainly the atomic charge of the nearest-neighbor O atoms changes. The atomic charges of the next nearest-neighboring Ce atoms change very little due to doping (cf. Fig. 4 and Table IV). The O atoms farther from the dopant in the c222 cell show atomic charges that differ only slightly from those in pure CeO_2.

Although all dopants are tetravalent the atomic charges vary significantly. The difference in atomic charge of the dopants and Ce is almost entirely compensated by the change in atomic charge on the nearest-neighbor O atoms, showing that even the nearby O–Ce bonds are barely affected by these dopants. For all group IV elements, the amount of noncom-

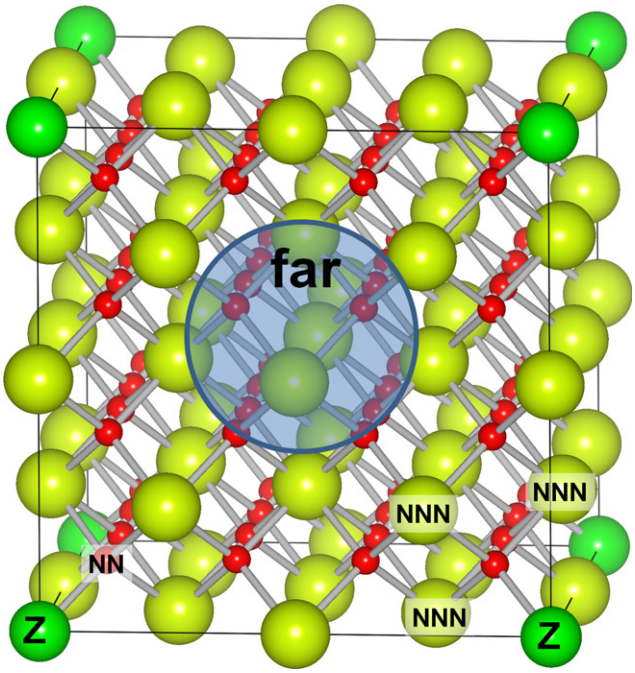

Fig. 4. Ball-and-stick model of a c222 CeO_2 supercell doped with 3.125% of a group IV element. The red/yellow/green balls give the positions of the O/Ce/dopant(Z) atoms. The nearest-neighbor O atom in one octant is labeled NN, whereas the next nearest neighboring Ce atoms in a single octant are labeled NNN. Atoms "far" away from the dopant are indicated by the blue disk.

pensated charge is less than 0.05*e* per O atom in the nearest-neighbor shell.

All dopants behave similarly, with carbon being the sole exception. This may be an indication of the much weaker bonds of the C atom with the surrounding O atoms than the other dopants, which is in agreement with the fact that the small C atom prefers short bonds. The small size of C (Shannon crystal radius[50,51] of 0.29 (0.3) Å for four (six) coordinated C) might make it very suited as an interstitial dopant or as substitutional dopant on an oxygen site, which are interesting scenarios for a study focussing on C doping of CeO_2, but are beyond the scope of this work.

Note, however, that even in the C case the effects remain localized to the C dopant and the surrounding O atoms in the nearest-neighbor shell. The fact that the C atom loses roughly two electrons less (i.e., the two electrons remain localized on the C atom) than the other dopants and Ce to the surrounding O atoms is consistent with the recent findings of Hellman *et al.*[52] They observed that for reduced C-doped ceria, the two electrons, which provided the formal charge of -II on the removed O atom, localize in C *p* orbitals.

From the results in Table IV, it appears that the group IV dopants cause no significant changes in the atomic charges beyond the nearest-neighbor shell.

III. Conclusion

Using *ab initio* DFT calculations we investigated the influence of tetravalent doping on the properties of fluorite CeO_2. On the basis of the calculated defect formation energies, we conclude that Ce-substitution with group IVa elements is rather unlikely, whereas group IVb elements are good substituents for tuning the CeO_2 fluorite lattice. This qualitative result is shown to be independent of the used functional and independent of the inclusion of a Coulomb correction.

Investigation of the DOS and LDOS for both high and low dopant concentrations shows that the presence of states in the O 2*p*–Ce 4*f* band gap are detrimental for the system. Low dopant concentration calculations show that group IVa dopants introduce localized gap states due to the overlap of their valence *s* states with the O 2*p* states of the surrounding O atoms. These gap states are connected to occupied atomic states below the O 2*p* band. These gap states also provide the means for excess electrons in reduced ceria to localize on the dopant. In case of the IVb elements, the gap state is always located above the unoccupied Ce 4*f* band resulting in a much reduced influence on the CeO_2 properties.

Comparison of the BM and the TEC shows that an inverse relation between these properties exists. Also here, group IVa and IVb elements differentiate, with group IVb elements resulting only in a slight increase in the BM, whereas a decrease in the BM is observed for group IVa dopants.

The influence of group IV dopants on the charge distribution of the systems is very limited, and it is shown that, despite significant changes at the nearest-neighbor atoms, no significant changes are observed farther away.

Throughout all results presented, the impact of the filled *d* and *f* shells located near the Fermi level is observed as oscillations in the presented trends that coincide with the introduction of a new shell. This shows that not only the outer valence electrons play a role, but also filled shells can promote significant modifications of the expected results.

Appendix A
Computational Details

We perform *ab-initio* spin-polarized DFT calculations using the projector augmented waves (PAWs) method as implemented in the Vienna *ab-initio* Package (VASP) program. The LDA functional as parameterized by Ceperley and Alder and the Generalized Gradient Approximation (GGA) functional as constructed by PBE are used to model the exchange and correlation behavior of the electrons.[53–58] This is sufficient for the mechanical and structural properties studied. To assess the influence of the strong on-site Coulomb repulsion between the Ce 4*f* electrons on electronic properties such as defect formation energy and DOS, calculations are also performed within the DFT + *U* level framework, as formulated by Duradev *et al.*[59] In different DFT + *U* studies, focussed on finding an optimum value for the Hubbard *U* parameter for ceria, a value for *U* of 5–6 and 4–5 eV is suggested for LDA and GGA, respectively.[37,60–62] For this reason we have chosen to use an on-site Coulomb repulsion with $U = 5$ eV for the Ce 4*f* electrons, for both LDA + *U* and PBE + *U* calculations. The plane wave kinetic energy cutoff is set to 500 eV.

Symmetric cells, containing a single substituent per cell are used to simulate a homogeneous distribution of dopants. Note that to have a clearer picture of the observed trends, C is also substituted at a Ce site and not at an O site, although this would be more in line with experimental expectations, as carbides of several rare earth elements, including cerium, are known.[63–65] For all systems, the fluorite symmetry (space group $Fm\bar{3}m$) is maintained allowing for straightforward correlation of the observed trends and the dopant atomic properties. The cells used are the fluorite cubic $1 \times 1 \times 1$ cell with 12 atoms (c111), the primitive $2 \times 2 \times 2$ cell with 24 atoms (p222), the primitive $3 \times 3 \times 3$ cell with 81 atoms (p333) and the cubic $2 \times 2 \times 2$ cell with 96 atoms (c222). Replacing a single Ce atom with a group IV element in these specific CeO_2 supercells results in dopant concentrations of 25, 12.5, 3.7037, and 3.125%, respectively.

The valence electron configurations considered in these systems are $5s^2\ 5p^6\ 6s^2\ 4f^1\ 5d^1$ for Ce and $2s^2\ 2p^4$ for O. For the group IVa dopants C and Si only the 4*s* and *p* valence electrons are considered, while 10 additional *d* electrons are included for Ge, Sn, and Pb. For the group IVb elements, the valence electron configurations considered are

Table V. Crystal Structure of the Reference Bulk and Oxide Materials Used

	Structure	Pearson symbol	Space group
C	Diamond	cF8	$Fd\bar{3}m$
Si	Diamond	cF8	$Fd\bar{3}m$
Ge	Diamond	cF8	$Fd\bar{3}m$
Sn	Diamond	cF8	$Fd\bar{3}m$
Pb	Face centered cubic	cF4	$Fm\bar{3}m$
Ti	Hexagonal close packed	hP2	$P63/mmc$
Zr	Hexagonal close packed	hP2	$P63/mmc$
Hf	Hexagonal close packed	hP2	$P63/mmc$
CO_2	Dry ice	cP12	$Pa\bar{3}$
SiO_2	α-quartz	cF8	$P3_121$
GeO_2	Rutile (argutite)	tP6	$P4_2/mnm$
SnO_2	Rutile (cassiterite)	tP6	$P4_2/mnm$
PbO_2	Rutile (plattnerite)	tP6	$P4_2/mnm$
TiO_2	Anatase	tI12	$I4_1/amd$
ZrO_2	Baddeleyite	mP12	$P12_1/c1$
HfO_2	Monoclinic(Baddeleyite)	mP12	$P12_1/c1$

$3p^6\ 4s^2\ 3d^2$, $4s^2\ 4p^6\ 5s^2\ 4d^2$, and $5p^6\ 6s^2\ 5d^2$ for Ti, Zr, and Hf, respectively. The crystal structure information of the reference bulk materials used for calculating defect formation energies is presented in Table V, since many of these systems can have more than one (meta-)stable crystal structure.

Monkhorst-Pack special k-point grids are used to sample the Brillouin zone.[66] For the two smaller cells we use an $8 \times 8 \times 8$ k-point grid while for the two large cells a $4 \times 4 \times 4$ k-point grid is used.

To optimize the structures, a conjugate gradient method is used. During relaxation both atomic positions and cell-geometry are allowed to change simultaneously. Convergence is obtained when the difference in energy between subsequent steps is smaller than 1.0×10^{-6} eV.

The thermal expansion coefficients (TECs) are calculated as the numerical derivative of $V(T)$ data. In turn, these $V(T)$ data are obtained through minimization of the thermal non-equilibrium Gibbs function, which is calculated using the quasi-harmonic Debye approximation, and is implemented as a module in our HIVE code.[67–70] The BM is calculated by fitting $E(V)$ data from fixed volume calculations to the third order isothermal Birch-Murnaghan equation of state.[71,72]

To calculate the atomic charges of the doped systems, we used the Hirshfeld-I approach.[47–49] Our implementation makes use of the grid stored pseudo-electron density distributions obtained from vasp. The atom centered spherical integrations are done using Lebedev–Laikov grids of 1202 grid points per shell, and a logarithmic radial grid.[73,74] The iterative scheme is considered converged when the largest difference in charge of a system atom is less than 1.0×10^{-5} electron in two consecutive iterations.

Appendix B
Oxide-Based Defect Formation Energies

The defect formation energy of doped ceria can also be calculated with regard to the dopant ZO_2 oxide (note that some group IV dopants, such as Pb, have multiple oxide stoichiometries). We chose to use ZO_2 type oxides since this corresponds to the stoichiometry of CeO_2 itself. Furthermore, since elements like Si have a large number of (meta-)stable oxide polymorphs with the ZO_2 stoichiometry, and since temperature and pressure effects are not included in the *ab initio* calculations, we opt for a low pressure/temperature structure as found in Ref. [75]. The oxide reference structures are shown in Table V. The defect formation energy, with regard to the oxides presented in Table V, is calculated as:

Table VI. Defect Formation Energy for Group IV Dopants at Different Concentrations, with Respect to the Dopant Oxides Mentioned

	E_f (eV)			
	25%	12.5%	3.704%	3.125%
	LDA			
CO_2	13.276	13.495	13.588	13.589
SiO_2	6.343	6.133	6.105	6.107
GeO_2	4.192	3.922	3.898	3.893
SnO_2	1.760	1.565	1.550	1.550
PbO_2	1.082	0.876	0.861	0.864
TiO_2	2.019	2.105	2.100	2.085
ZrO_2	0.419	0.444	0.437	0.432
HfO_2	0.706	0.740	0.732	0.730
	PBE			
CO_2	13.353	13.556	13.620	13.633
SiO_2	6.727	6.537	6.520	6.552
GeO_2	3.936	3.698	3.683	3.695
SnO_2	1.714	1.551	1.546	1.545
PbO_2	1.085	0.913	0.903	0.905
TiO_2	2.164	2.236	2.234	2.242
ZrO_2	0.554	0.587	0.588	0.586
HfO_2	0.765	0.798	0.798	0.798

$$E_f^{ZO_2} = E_{Ce_{1-x}Z_xO_2} + (x-1)E_{CeO_2} - xE_{ZO_2} \quad (2)$$

with $E_{Ce_{1-x}Z_xO_2}$ the total energy of the doped system, E_{CeO_2} the total energy of bulk CeO_2 and E_{ZO_2} the bulk energy of the oxide ZO_2 (with Z = C, Si, Ge, Sn, Pb, Ti, Zr, and Hf). The resulting energies are shown in Table VI. The same general trends are observed as for the defect formation energy presented in the manuscript: (a) little concentration dependence, (b) large range of energies depending on the dopant element, and (c) none of the dopants improve the stability of CeO_2. The obtained energies, however, are lower due to the increased stability of the formed oxides. This means that for experiments, starting from the oxides, it will be easier to form group IV-doped CeO_2, then if one would start with the bulk dopant material.

Acknowledgment

This research was financially supported by FWO-Vlaanderen, project no. G. 0802.09N. We also acknowledge the Research Board of Ghent University. All calculations were carried out using the Stevin Supercomputer Infrastructure at Ghent University.

References

[1]A. Trovarelli, "Catalytic Properties of Ceria and CeO_2-Containing Materials," *Catal. Rev. – Sci. Eng.*, **38** [4] 439–520 (1996).
[2]J. Kašpar, P. Fornasiero, and M. Graziani, "Use of CeO_2-Based Oxides in the Three-Way Catalysis," *Catal. Today*, **50** [2] 285–98 (1999).
[3]Q. Fu, H. Saltsburg, and M. Flytzani-Stephanopoulos, "Active Nonmetallic Au and Pt Species on Ceria-Based Water-Gas Shift Catalysts," *Science*, **301** [5635] 935–8 (2003).
[4]Y. She, Q. Zheng, L. Li, Y. Zhan, C. Chen, Y. Zheng, and X. Lin, "Rare Earth Oxide Modified CuO/CeO_2 Catalysts for the Water–Gas Shift Reaction," *Int. J. Hydrogen Energy*, **34** [21] 8929–36 (2009).
[5]C. De Leitenburg, A. Trovarelli, F. Zamar, S. Maschio, G. Dolcetti, and J. Llorca, "A Novel and Simple Route to Catalysts With a High Oxygen Storage Capacity – the Direct Room-Temperature Synthesis of CeO_2–ZrO_2 Solid Solutions," *J. Chem. Soc., Chem. Commun.*, **21**, 2181–2 (1995).
[6]L. Kundakovic and M. Flytzani-Stephanopoulos, "Cu- and Ag-Modified Cerium Oxide Catalysts for Methane Oxidation," *J. Catal.*, **179** [1] 203–21 (1998).
[7]M. Manzoli, G. Avgouropoulos, T. Tabakova, J. Papavasiliou, T. Ioannides, and F. Boccuzzi, "Preferential CO Oxidation in H_2-Rich gas Mixtures Over Au/Doped Ceria Catalysts," *Catal. Today*, **138** [3–4] 239–43 (2008).

[8]B. Li, X. Wei, and W. Pan, "Improved Electrical Conductivity of $Ce_{0.9}Gd_{0.1}O_{1.95}$ and $Ce_{0.9}Sm_{0.1}O_{1.95}$ by Co-Doping," *Int. J. Hydrogen Energy*, **35** [7] 3018–22 (2010).
[9]D. E. P. Vanpoucke, P. Bultinck, S. Cottenier, V. Van Speybroeck, and I. Van Driessche, "Density Functional Theory Study of $La_2Ce_2O_7$: Disordered Fluorite Versus Pyrochlore Structure," *Phys. Rev. B*, **84** [5] 054110, 9pp (2011).
[10]M. Paranthaman, A. Goyal, F. List, E. Specht, D. Lee, P. Martin, Q. He, D. Christen, D. Norton, J. Budai, and D. Kroeger, "Growth of Biaxially Textured Buffer Layers on Rolled-Ni Substrates by Electron Beam Evaporation," *Phys. C*, **275** [3–4] 266–72 (1997).
[11]S. Oh, J. Yoo, K. Lee, J. Kim, and D. Youm, "Comparative Study on the Crack Formations in the CeO_2 Buffer Layers for YBCO Films on Textured Ni Tapes and Pt Tapes," *Phys. C*, **308** [1–2] 91–8 (1998).
[12]G. Penneman, I. Van Driessche, E. Bruneel, and S. Hoste, "Deposition of CeO_2 Buffer Layers and $YBa_2Cu_3O_{7-\delta}$ Superconducting Layers Using an Aqueous sol-gel Method"; pp. 501–4 in *Key Engineering Materials*, Vol. 264–268, Euro Ceramics VIII, Pts 1-3, Edited by H. Mandal and L. Ovecoglu. Turkish Ceram Soc, European Ceram Soc, Zurich, 2004.
[13]Y. Takahashi, Y. Aoki, T. Hasegawa, T. Maeda, T. Honjo, Y. Yamada, and Y. Shiohara, "Preparation of YBCO Coated Conductor on Metallic Tapes Using an MOD Process," *Phys. C*, **412–414** [2] 905–9 (2004).
[14]K. Knoth, B. Schlobach, R. Hühne, L. Schultz, and B. Holzapfel, "$La_2Zr_2O_7$ and Ce–Gd–O Buffer Layers for YBCO Coated Conductors Using Chemical Solution Deposition," *Phys. C*, **426–431** [2] 979–84 (2005).
[15]N. Van de Velde, D. Van de Vyver, O. Brunkahl, S. Hoste, E. Bruneel, and I. Van Driessche, "CeO_2 Buffer Layers for HTSC by an Aqueous Sol-Gel Method – Chemistry and Microstructure," *Eur. J. Inorg. Chem.*, **2010** [2] 233–41 (2010).
[16]V. Narayanan, P. Lommens, K. De Buysser, D. E. P. Vanpoucke, R. Huehne, L. Molina, G. Van Tendeloo, P. Van Der Voort, and I. Van Driessche, "Aqueous CSD Approach for the Growth of Novel, Lattice-Tuned $La_xCe_{1-x}O_\delta$ Epitaxial Layers," *J. Mater. Chem.*, **22** [17] 8476–83 (2012).
[17]M. Mogensen, N. M. Sammes, and G. A. Tompsett, "Physical, Chemical, and Electrochemical Properties of Pure and Doped Ceria," *Solid State Ionics*, **129** [1–4] 63–94 (2000).
[18]T. Kudo and H. Obayashi, "Oxygen Ion Conduction of the Fluorite-Type $Ce_{1-x}Ln_xO_{2-x/2}$ (Ln = Lanthanoid Element)," *J. Electrochem. Soc.*, **122** [1] 142–7 (1975).
[19]J. R. McBride, K. C. Hass, B. D. Poindexter, and W. H. Weber, "Raman and X-Ray Studies of $Ce_{1-x}RE_xO_{2-y}$, Where RE = La, Pr, Nd, Eu, Gd, and Tb," *J. Appl. Phys.*, **76** [4] 2435–41 (1994).
[20]L. Kundakovic and M. Flytzani-Stephanopoulos, "Reduction Characteristics of Copper Oxide in Cerium and Zirconium Oxide Systems," *Appl. Catal. A*, **171** [1] 13–29 (1998).
[21]S. Rossignol, F. Gerard, and D. Duprez, "Effect of the Preparation Method on the Properties of Zirconia-Ceria Materials," *J. Mater. Chem.*, **9** [7] 1615–20 (1999).
[22]P. Bera, K. R. Priolkar, P. R. Sarode, M. S. Hegde, S. Emura, R. Kumashiro, and N. P. Lalla, "Structural Investigation of Combustion Synthesized Cu/CeO_2 Catalysts by EXAFS and Other Physical Techniques: Formation of a $Ce_{1-x}Cu_xO_{2-\delta}$ Solid Solution," *Chem. Mater.*, **14** [8] 3591–601 (2002).
[23]H. Yamamura, H. Nishino, K. Kakinuma, and K. Nomura, "Crystal Phase and Electrical Conductivity in the Pyrochlore-Type Composition Systems, $Ln_2Ce_2O_7$ (Ln = La, Nd, Sm, Eu, Gd, Y and Yb)," *J. Ceram. Soc. Jpn.*, **111** [12] 902–6 (2003).
[24]X. Wang, J. A. Rodriguez, J. C. Hanson, D. Gamarra, A. Martínez-Arias, and M. Fernández-García, "Unusual Physical and Chemical Properties of Cu in $Ce_{1-x}Cu_xO_2$ Oxides," *J. Phys. Chem. B*, **109** [42] 19595–603 (2005).
[25]D. Fagg, J. Frade, V. Kharton, and I. Marozau, "The Defect Chemistry of $Ce(Pr, Zr)O_{2-\delta}$," *J. Solid State Chem.*, **179** [5] 1469–77 (2006).
[26]A. Tiwari, V. M. Bhosle, S. Ramachandran, N. Sudhakar, J. Narayan, S. Budak, and A. Gupta, "Ferromagnetism in Co Doped CeO_2: Observation of a Giant Magnetic Moment With a High Curie Temperature," *Appl. Phys. Lett.*, **88** [14] 142511, 3pp (2006).
[27]A. Nakamura, N. Masaki, H. Otobe, Y. Hinatsu, J. Wang, and M. Takeda, "Defect-Fluorite Oxides $M_{1-y}Ln_yO_{2-y/2}$ (Ln = Lanthanide; M = Hf, Zr, Ce, U, Th): Structure, Property, and Applications," *Pure Appl. Chem.*, **79** [10] 1691–729 (2007).
[28]Y. Q. Song, H. W. Zhang, Q. Y. Wen, H. Zhu, and J. Q. Xiao, "Co Doping Effect on the Magnetic Properties of CeO_2 Films on Si(111) Substrates," *J. Appl. Phys.*, **102** [4] 043912, 5pp (2007).
[29]B. Vodungbo, Y. Zheng, F. Vidal, D. Demaille, V. H. Etgens, and D. H. Mosca, "Room Temperature Ferromagnetism of Co Doped $CeO_{2-\delta}$ Diluted Magnetic Oxide: Effect of Oxygen and Anisotropy," *Appl. Phys. Lett.*, **90** [6] 062510, 3pp (2007).
[30]R. de Biasi and M. Grillo, "Evidence for Clustering in Cu^{2+}-Doped CeO_2," *J. Alloy. Compd.*, **462** [1–2] 15–8 (2008).
[31]R. K. Singhal, P. Kumari, S. Kumar, S. N. Dolia, Y. T. Xing, M. Alzamora, U. P. Deshpande, T. Shripathi, and E. Saitovitch, "Room Temperature Ferromagnetism in Pure and Co- and Fe-Doped CeO_2 Dilute Magnetic Oxide: Effect of Oxygen Vacancies and Cation Valence," *J. Phys. D: Appl. Phys.*, **44** [16] 165002, 3pp (2011).
[32]B. M. Reddy, A. Khan, P. Lakshmanan, M. Aouine, S. Loridant, and J.-C. Volta, "Structural Characterization of Nanosized CeO_2–SiO_2, CeO_2–TiO_2, and CeO_2–ZrO_2 Catalysts by XRD, Raman, and HREM Techniques," *J. Phys. Chem. B*, **109** [8] 3355–63 (2005).
[33]B. Reddy and A. Khan, "Nanosized CeO_2–SiO_2, CeO_2–TiO_2, and CeO_2–ZrO_2 Mixed Oxides: Influence of Supporting Oxide on Thermal Stability and Oxygen Storage Properties of Ceria," *Catal. Surv. Asia*, **9** [3] 155–71 (2005).
[34]E. Rocchini, A. Trovarelli, J. Llorca, G. W. Graham, W. H. Weber, M. Maciejewski, and A. Baiker, "Relationships Between Structural/Morphological Modifications and Oxygen Storage–Redox Behavior of Silica-Doped Ceria," *J. Catal.*, **194** [2] 461–78 (2000).
[35]E. Rocchini, M. Vicario, J. Llorca, C. de Leitenburg, G. Dolcetti, and A. Trovarelli, "Reduction and Oxygen Storage Behavior of Noble Metals Supported on Silica-Doped Ceria," *J. Catal.*, **211** [2] 407–21 (2002).
[36]R. Lin, M.-F. Luo, Y.-J. Zhong, Z.-L. Yan, G.-Y. Liu, and W.-P. Liu, "Comparative Study of $CuO/Ce_{0.7}Sn_{0.3}O_2$, CuO/CeO_2 and CuO/SnO_2 Catalysts for low-Temperature CO Oxidation," *Appl. Catal. A*, **255** [2] 331–6 (2003).
[37]D. A. Andersson, S. I. Simak, N. V. Skorodumova, I. A. Abrikosov, and B. Johansson, "Theoretical Study of CeO_2 Doped With Tetravalent Ions," *Phys. Rev. B*, **76** [17] 174119, 10pp (2007).
[38]D. A. Andersson, S. I. Simak, N. V. Skorodumova, I. A. Abrikosov, and B. Johansson, "Redox Properties of CeO_2–MO_2 (M = Ti, Zr, Hf, or Th) Solid Solutions From First Principles Calculations," *Appl. Phys. Lett.*, **90** [3] 031909, 3pp (2007).
[39]Y. Tang, H. Zhang, L. Cui, C. Ouyang, S. Shi, W. Tang, H. Li, J.-S. Lee, and L. Chen, "First-Principles Investigation on Redox Properties of m-Doped CeO_2 (m = Mn, Pr, Sn, Zr)," *Phys. Rev. B*, **82** [12] 125104, 9pp (2010).
[40]M. Yashima, "Crystal Structures of the Tetragonal Ceria–Zirconia Solid Solutions $Ce_xZr_{1-x}O_2$ Through First Principles Calculations ($0 \le x \le 1$)," *J. Phys. Chem. C*, **113** [29] 12658–62 (2009).
[41]D. E. P. Vanpoucke, S. Cottenier, V. Van Speybroeck, P. Bultinck, and I. Van Driessche, "Tuning of CeO_2 Buffer Layers for Coated Superconductors Through Doping," *Appl. Surf. Sci.*, **260**, 32–5 (2012).
[42]D. A. Andersson, S. I. Simak, B. Johansson, I. A. Abrikosov, and N. V. Skorodumova, "Modeling of CeO_2, Ce_2O_3, and CeO_{2-x} in the LDA + U Formalism," *Phys. Rev. B*, **75** [3] 035109, 6pp (2007).
[43]M. V. Ganduglia-Pirovano, A. Hofmann, and J. Sauer, "Oxygen Vacancies in Transition Metal and Rare Earth Oxides: Current State of Understanding and Remaining Challenges," *Surf. Sci. Rep.*, **62** [6] 219–70 (2007).
[44]M. Panhans and R. Blumenthal, "A Thermodynamic and Electrical Conductivity Study of Nonstoichiometric Cerium Dioxide," *Solid State Ionics*, **60** [4] 279–98 (1993).
[45]C. Kittel, *Introduction to Solid State Physics*, pp. 57, 7th edition, Edited by S. Johnson and P. McFadden. John Wiley and Sons, Inc., New York, 1996.
[46]Y. Tsuru, Y. Shinzato, Y. Saito, M. Shimazu, M. Shiono, and M. Morinaga, "Estimation of Linear Thermal Expansion Coefficient from Cohesive Energy Obtained by *Ab Initio* Calculation of Metals and Ceramics," *J. Ceram. Soc. Jpn.*, **118** [1375] 241–5 (2010).
[47]P. Bultinck, C. Van Alsenoy, P. W. Ayers, and R. Carbó-Dorca, "Critical Analysis and Extension of the Hirshfeld Atoms in Molecules," *J. Chem. Phys.*, **126** [14] 144111, 9pp (2007).
[48]D. E. P. Vanpoucke, P. Bultinck, and I. Van Driessche, "Extending Hirshfeld-I to Bulk and Periodic Materials," *J. Comput. Chem.*, **34** [5] 405–17 (2013).
[49]D. E. P. Vanpoucke, I. Van Driessche, and P. Bultinck, "Reply to Comment on "Extending Hirshfeld-I to Bulk and Periodic Materials"," *J. Comput. Chem.*, **34** [5] 422–7 (2013).
[50]R. D. Shannon, "Revised Effective Ionic Radii and Systematic Studies of Interatomic Distances in Halides and Chalcogenides," *Acta Crystallogr.*, **32** 751–67 (1976).
[51]J. D. Van Horn, "Electronic Table of Shannon Ionic Radii." (2001). http://v.web.umkc.edu/vanhornj/shannonradii.htm 08/13/2010.
[52]O. Hellman, N. V. Skorodumova, and S. I. Simak, "Charge Redistribution Mechanisms of Ceria Reduction," *Phys. Rev. Lett.*, **108** [13] 135504, 4pp (2012).
[53]P. E. Blöchl, "Projector Augmented-Wave Method," *Phys. Rev. B*, **50** [24] 17953–79 (1994).
[54]G. Kresse and D. Joubert, "From Ultrasoft Pseudopotentials to the Projector Augmented-Wave Method," *Phys. Rev. B*, **59** [3] 1758–75 (1999).
[55]D. M. Ceperley and B. J. Alder, "Ground State of the Electron Gas by a Stochastic Method," *Phys. Rev. Lett.*, **45** [7] 566–9 (1980).
[56]J. P. Perdew, K. Burke, and M. Ernzerhof, "Generalized Gradient Approximation Made Simple," *Phys. Rev. Lett.*, **77** [18] 3865–8 (1996).
[57]G. Kresse and J. Hafner, "*Ab Initio* Molecular Dynamics for Liquid Metals," *Phys. Rev. B*, **47** [1] 558–61 (1993).
[58]G. Kresse and J. Furthmüller, "Efficient Iterative Schemes for *ab Initio* Total-Energy Calculations Using a Plane-Wave Basis set," *Phys. Rev. B*, **54** [16] 11169–86 (1996).
[59]S. L. Dudarev, G. A. Botton, S. Y. Savrasov, C. J. Humphreys, and A. P. Sutton, "Electron-Energy-Loss Spectra and the Structural Stability of Nickel Oxide: An LSDA + U Study," *Phys. Rev. B*, **57** [3] 1505–9 (1998).
[60]C. Loschen, J. Carrasco, K. M. Neyman, and F. Illas, "First-Principles LDA + U and GGA + U Study of Cerium Oxides: Dependence on the Effective U Parameter," *Phys. Rev. B*, **75** [3] 035115, 8pp (2007).
[61]C. W. M. Castleton, J. Kullgren, and K. Hermansson, "Tuning LDA + U for Electron Localization and Structure at Oxygen Vacancies in Ceria," *J. Chem. Phys.*, **127** [24] 244704, 11pp (2007).
[62]J. L. F. Da Silva, "Stability of the Ce_2O_3 Phases: A DFT + U Investigation," *Phys. Rev. B*, **76** [19] 193108, 4pp (2007).
[63]F. H. Spedding, K. Gschneidner, and A. H. Daane, "The Crystal Structures of Some of the Rare Earth Carbides," *J. Am. Chem. Soc.*, **80** [17] 4499–503 (1958).
[64]G.-Y. Adachi, T. Nishihata, and J. Shiokawa, "Rare-Earth Mixed Dicarbides," *J. Less-Common Met.*, **32** [2] 301–6 (1973).

[65]T. Sakai, G.-Y. Adachi, T. Yoshida, and J. Shiokawa, "Magnetic and Electrical Properties of Rare Earth Dicarbides and Their Solid Solutions," *J. Less-Common Met.*, **81** [1] 91–102 (1981).
[66]H. J. Monkhorst and J. D. Pack, "Special Points for Brillouin-Zone Integrations," *Phys. Rev. B*, **13** [12] 5188–92 (1976).
[67]A. A. Maradudin, E. W. Montroll, G. H. Weiss, and I. P. Ipatova, *Theory of Lattice Dynamics in the Harmonic Approximation*. 2nd edition, Academic press, New York, 1971.
[68]M. A. Blanco, A. M. Pendas, E. Francisco, J. M. Recio, and R. Franco, "Thermodynamical Properties of Solids From Microscopic Theory: Applications to MgF_2 and Al_2O_3," *J. Mol. Struct. (Thoechem)*, **368**, 245–55 (1996).
[69]E. Francisco, M. A. Blanco, and G. Sanjurjo, "Atomistic Simulation of SrF_2 Polymorphs," *Phys. Rev. B*, **63** [9] 094107, 9pp (2001).
[70]D. E. P. Vanpoucke, "HIVE v2.1." (2011). http://users.ugent.be/~devpouck.
[71]F. D. Murnaghan, "The Compressibility of Media Under Extreme Pressures," *Proc. Natl. Acad. Sci. USA*, **30** [9] 244–7 (1944).
[72]F. Birch, "Finite Elastic Strain of Cubic Crystals," *Phys. Rev.*, **71** [11] 809–24 (1947).
[73]A. D. Becke, "A Multicenter Numerical Integration Scheme for Polyatomic Molecules," *J. Chem. Phys.*, **88** [4] 2547–53 (1988).
[74]V. I. Lebedev and D. Laikov, "Quadrature Formula for the Sphere of 131-th Algebraic Order of Accuracy," *Dokl. Math.*, **59** [3] 477–81 (1999).
[75]L. Merrill, "Behavior of the AB_2-Type Compounds at High Pressures and High Temperatures," *J. Phys. Chem. Ref. Data*, **11** [4] 1005–64 (1982). □